Xu et al. *Zool. Res.* 2026, 47(2): 561−576
https://doi.org/10.24272/j.issn.2095-8137.2025.190
https://cstr.cn/32248.14.zr.2025.190

ZR | Zoological Research

Article Open Access

Integrative single-cell RNA-seq and ATAC-seq profiling identifies NTN5$^+$LSAMP$^+$ myoblasts as mediators of impaired embryonic myogenesis

Rong Xu[1,#], Xiao-Yu Wang[1,#], Zhi-Ting Feng[1], Shu-Fang Cai[1], Zi-Yun Liang[1], Li-Ping Pan[1], Qing-Shuang Zhou[1], Xiao-Hong Liu[1], Yao-Sheng Chen[1], De-Lin Mo[1,*]

[1] *State Key Laboratory of Biocontrol*, *School of Life Sciences*, *Sun Yat-sen University*, *Guangzhou*, *Guangdong* 510275, *China*

ABSTRACT

Prenatal myogenesis establishes the cellular and regulatory framework that determines postnatal muscle mass and contractile performance, and represents a critical period for elucidating mechanisms underlying developmental myopathies and impaired fetal growth. In this study, integrated single-cell transcriptomic and chromatin accessibility profiling was applied to compare the regulatory landscapes between growth-restricted and normal porcine embryonic somites. This analysis uncovered a distinct pathogenic myoblast population characterized by co-expression of netrin-5 (*NTN5*) and limbic system-associated membrane protein (*LSAMP*), markedly enriched in growth-restricted embryos. These NTN5$^+$LSAMP$^+$ myoblasts exhibited a cell-autonomous differentiation blockade accompanied by coordinated epigenetic and metabolic dysregulation. Chromatin landscapes revealed sustained accessibility at the cytoskeletal regulator tropomyosin-3 (*TPM3*), suppressed accessibility at the muscle-specific actin depolymerization factor cofilin-2 (*CFL2*), and transcriptional programs consistent with impaired glycolytic flux. Perturbation of the Hippo/TGF-β signaling pathway, together with disrupted ligand–receptor interactions, exacerbated the differentiation arrest. Reconstruction of a multi-omics regulatory network delineated the mechanisms underlying aberrant embryonic myogenesis, identifying *NTN5* and *LSAMP* as key regulators of porcine skeletal muscle development. Collectively, these findings define mechanistic determinants of impaired fetal myogenesis and provide candidate targets for therapeutic intervention in growth restriction as well as molecular strategies for optimizing muscle accretion in livestock.

Keywords: Pig; Differentiation arrest; Skeletal muscle development; *NTN5*; *LSAMP*

INTRODUCTION

Skeletal muscle accounts for approximately 40% of total body weight and is indispensable for locomotion, metabolic homeostasis, and systemic physiological stability (Frontera & Ochala, 2015). During embryogenesis, skeletal myogenesis proceeds through two sequential phases. Myogenic progenitors arise from paraxial mesoderm and undergo proliferation, differentiation, and fusion to form primary myofibers. Subsequently, fetal myoblasts expand and utilize primary myofibers as structural scaffolds, fusing either with existing fibers or with one another to form secondary myofibers (Bentzinger et al., 2012; Chal & Pourquié, 2017; Picard et al., 2002). The total number of muscle fibers (TNF) is largely established at birth, after which postnatal muscle growth occurs through hypertrophic enlargement of individual myofibers rather than through additional fiber formation (Picard et al., 2002; Schiaffino et al., 2013). In livestock species, embryonic myofiber formation is a key determinant of postnatal muscle mass and ultimately influences meat production efficiency.

Embryonic skeletal myogenesis unfolds through a hierarchically organized transcriptional network centered on paired box (Pax) proteins and myogenic regulatory factors (MRFs) (Bentzinger et al., 2012; Parker et al., 2003; Tajbakhsh, 2009). *Pax3* and its paralog *Pax7*, as markers of myogenic precursors, function as critical upstream regulators that establish myogenic competence (Bober et al., 1994; Buckingham & Relaix, 2015; Relaix et al., 2006; Schubert et al., 2001; Seale et al., 2000). The MRF family, consisting of MyoD, Myf5, myogenin, and Mrf4 (Myf6), shares a basic helix-loop-helix (bHLH) domain to control myogenesis. During early

Received: 08 July 2025; Accepted: 15 September 2025; Online: 16 September 2025

Foundation items: This work was supported by the National Natural Science Foundation of China (32472858, 32072697), Selection and Breeding of New Local Pig Breeds and Promotion of Industrialization (2024-XPY-00-001), Modern Agricultural Industrial Technology System Innovation Team of Guangdong Province (2024CXTD22), and Earmarked Fund for CARS-35

[#]Authors contributed equally to this work

*Corresponding author, E-mail: modelin@mail.sysu.edu.cn

embryonic stages, Myf5 and MyoD initiate myogenic differentiation and activate the transcriptional program that drives commitment toward the muscle lineage. At later stages, myogenin and Mrf4 participate in terminal differentiation, myoblast fusion, and structural maturation of myofibers (Bentzinger et al., 2012; Parker et al., 2003; Pownall et al., 2002).

Healthy skeletal muscle development requires precise spatiotemporal regulation of intercellular signaling cascades and stage-specific transcriptional programs. Dysregulation of these regulatory networks drives a broad spectrum of congenital and acquired myopathies. Becker muscular dystrophy and Duchenne muscular dystrophy represent the most common inherited forms and arise from mutations in the dystrophin gene (Bez Batti Angulski et al., 2023; Findlay & Weihl, 2022). Mutations in MET impair embryonic muscle development by inhibiting migration of myogenic progenitor cells and reducing proliferation of secondary myoblasts (Zhou et al., 2019). Defects in lamin A/C give rise to diverse subtypes of congenital muscular dystrophy (Butterfield, 2019). Additional categories, including distal, oculopharyngeal, and limb-girdle muscular dystrophies, result from heterogeneous genetic lesions and exhibit distinct clinical phenotypes (Emery, 2002). Given the anatomical and physiological similarities between porcine and human musculoskeletal systems, pigs provide a powerful preclinical platform for modeling genetic muscle disorders (Lunney et al., 2021; Stirm et al., 2022). As a major agricultural species, pigs further offer a dual translational framework in which mechanistic insights into myogenesis inform both biomedical research and strategies to enhance meat production efficiency. This convergence of medical and agricultural priorities necessitates comprehensive dissection of regulatory mechanisms governing porcine skeletal muscle development.

Single-cell RNA sequencing (scRNA-seq) has transformed resolution of cellular heterogeneity and enabled systematic characterization of molecular mechanisms underlying complex pathologies (Stuart & Satija, 2019; Zhang et al., 2022). Application of this technology to skeletal muscle has revealed unexpected diversity within muscle-resident populations. De Micheli et al. (2020) identified 16 transcriptionally distinct cell populations in human skeletal muscle and defined spatially resolved transcriptional signatures of activated muscle stem cells (MuSCs) and niche-resident progenitors. Furthermore, Xu et al. (2023) employed single-cell transcriptomics to examine artificial selection-driven remodeling of muscle-resident cellular niches in swine, revealing evolutionary constraints on myogenic adaptation. Analysis of fibro/adipogenic progenitors (FAPs) in healthy and diseased murine muscle further clarified contributions of these cells to muscular pathology (Uapinyoying et al., 2023). Despite these advances, the influence of genetic background on embryonic myogenic regulation remains insufficiently explored.

In the present study, integrated single-cell transcriptomic and chromatin accessibility profiling was applied to compare patterns of developmental dysregulation during embryonic myogenesis in growth-restricted and healthy pig embryos from the same litter at embryonic day 21 (E21), a critical period for early myogenic commitment and initiation of myogenic gene expression (Cai et al., 2023b). An $NTN5^{+}LSAMP^{+}$ myoblast subpopulation associated with growth restriction was identified, characterized by epigenetic and metabolic programs that constrained progression beyond a lineage-committed blockade state. Coupling chromatin accessibility landscapes with dysregulated IGF1, Hippo, and TGF-β signaling pathways revealed embryonic chromatin architecture as a central determinant of muscle developmental trajectory. These findings establish a regulatory framework for understanding impaired fetal myogenesis and provide molecular targets with potential utility in precision breeding strategies.

MATERIALS AND METHODS

Animal study

Artificial insemination was performed on Xizang sows using semen obtained from Duroc boars. Semen was collected and evaluated for motility and morphological integrity prior to use. Following detection of estrus, diluted semen was administered 48 h later. The insemination procedure involved gentle restraint, perineal disinfection, and deposition of semen into the uterine horn. Pregnant females were then single-housed and monitored daily to ensure health and welfare. Food and water were provided *ad libitum*. At embryonic day 21 (E21), growth-restricted and phenotypically normal embryos were collected from the same sow under anesthesia. Throughout the study, strict adherence to animal welfare standards was maintained and all efforts were made to minimize stress and discomfort. All experimental procedures complied with the National Research Council Guide for the Care and Use of Laboratory Animals and received approval from the Institutional Animal Care and Use Committee of Sun Yat-sen University (Approval No.: SYSU-IACUC-2023-B0631).

Single-cell suspension preparation

Somite tissues were isolated from Duroc×Xizang hybrid embryos at E21 and rinsed three times with pre-cooled phosphate-buffered saline (PBS). Tissues were minced into small pieces and transferred into pre-warmed digestion medium consisting of RPMI 1640 supplemented with 0.1 mg/mL collagenase I (Sigma-Aldrich, USA) and 100 μg/mL DNase I (Sigma-Aldrich, USA). Enzymatic dissociation into single-cell suspensions was performed according to established protocols (Cai et al., 2023b). Briefly, tissues were digested in an incubator at 37°C for 45 min with agitation every 5 min to facilitate cellular release. The resulting suspension was filtered through a 70 μm cell strainer (BD Biosciences, USA) and transferred to a 15 mL centrifuge tube. Cells were pelleted by centrifugation at 500 ×*g* for 5 min at room temperature, after which the supernatant was discarded, and the pellet was washed with PBS. Cell viability was assessed using Trypan Blue staining (Thermo Fisher, USA) and quantified with an automated cell counter (Countstar, China).

Generation of 10x Genomics scRNA-seq libraries and sequencing

Single-cell suspensions were processed using the 10x Genomics Single Cell 3' Reagent Kit (v2) according to the manufacturer guidelines to generate barcoded water-in-oil droplets. Reverse transcription and cDNA amplification were performed using a Veriti 96-well thermal cycler (Thermo Fisher, USA). Amplified cDNA was then purified with SPRIselect magnetic beads (Beckman, USA) and assessed using a bioanalyzer to determine concentration and fragment distribution. cDNA libraries were constructed following the Single Cell 3' Reagent Kit (v3) user guide.

Quality control for scRNA-seq

Raw sequencing data were aligned to the porcine reference genome (Sscrofa 11.1) using Cell Ranger (10x Genomics, USA) to generate gene expression matrices for each sample. Unique molecular identifier (UMI) counts for each gene per cell were processed using R (v.3.5.2, https://www.R-project.org/). Quality filtering criteria for cells and genes were defined as follows: cells with fewer than 200 detected genes or more than 30 000 UMIs were removed; cells with more than 10% mitochondrial gene reads were excluded. The 10% mitochondrial threshold was selected based on prior analysis to enable joint dataset integration (Cai et al., 2023b) and is widely applied to balance removal of damaged cells with retention of biologically informative populations (Osorio & Cai, 2021; Subramanian et al., 2022; Xu et al., 2023). To reduce doublet contamination, cells flagged by DoubletFinder (McGinnis et al., 2019) and exhibiting more than 20 000 transcripts were discarded. Furthermore, genes detected in fewer than three cells, defined by UMI counts greater than zero, were also removed. After quality control filtering, a total of 21 350 high-quality cells were retained for further analysis.

Cell clustering and cell type annotation

Dimensionality reduction, unsupervised clustering, and visualization of scRNA-seq data were conducted using Seurat (v.4.0) under default settings. Cross-sample integration was achieved using canonical correlation analysis (CCA)-based anchor identification. Principal component analysis (PCA) was conducted, and the top 20 principal components (PCs) were selected for downstream analyses. Cell clustering was implemented using the Louvain community detection algorithm with a resolution parameter of 0.6, yielding 20 transcriptionally distinct clusters. Differentially expressed genes (DEGs) were identified using the Wilcoxon rank-sum test according to the following criteria: detection in at least 10% of cells within a minimum of one cluster; absolute log-fold change of at least 0.25; and Benjamini-Hochberg (BH)-adjusted P<0.05. Cell identities were assigned manually based on established marker genes, producing 11 cell populations for subsequent analyses.

Gene function analysis

Functional enrichment analysis was conducted on highly differentially expressed genes within each cell population using Gene Ontology (GO) annotation. Enrichment was evaluated across three ontological domains: cellular component (CC), biological process (BP), and molecular function (MF). All associated GO terms were retrieved, and statistical significance was assessed using Fisher's exact test. Terms with P<0.05 were considered significantly enriched.

Ligand-receptor interactions

Cell-cell communication among myogenic subsets was inferred using CellPhoneDB under default parameters. Ligand-receptor pairs with P<0.05 were regarded as statistically significant.

ScRNA-seq trajectory analysis

Pseudotemporal ordering of myogenic populations was reconstructed using Monocle2 (Qiu et al., 2017). Dimensionality reduction was performed using the "reduceDimension" function, and cells were arranged along developmental trajectories using "orderCells" with the DDRTree algorithm.

Single-cell assay for transposase-accessible chromatin sequencing (scATAC-seq)

Sample preparation, library construction, and sequencing for scATAC-seq were conducted using the Chromium Single-Cell ATAC Library & Gel Bead Kit according to manufacturer guidelines. Raw scATAC-seq data were processed and analyzed using ArchR.

Cell filtering and clustering

Raw sequencing reads were subjected to quality filtering using Fastp (https://github.com/OpenGene/fastp) under default parameters to remove low-quality reads and adapter contamination. The scATAC-seq data were processed with ArchR (https://www.archrproject.com/), and low-quality cells were excluded based on the following criteria: unique nuclear fragments (nFrags)≥1 000 and transcription start site enrichment scores≥4 for each library. Doublet scores were calculated using the "addDoubletScores" function with filterRatio set to 2, and predicted doublets were removed based on ArchR guidelines. Dimensionality reduction was performed independently for each sample using iterative latent semantic indexing (LSI) implemented in the "addIterativeLSI" function. Cell clustering was performed using the "FindClusters" function with the following parameters: reducedDims="IterativeLSI", method="Seurat", and resolution=0.8. Cluster-specific marker features were identified using the "getMarkerFeatures" function with thresholds of false discovery rate (FDR)≤0.05 and $\log_2$fold change≥0.25.

Identification of differentially accessible peaks

Accessible chromatin regions were considered differentially accessible if detected in at least 10% of cells within one group and exhibiting a log fold change of at least 0.25 between groups. Differential testing was performed using the "FindMarkers" function with BH-adjusted P<0.05 and the latent variable specified as "peak_region_fragments".

ScATAC-seq trajectory analysis

Cell trajectories were constructed using the "addTrajectory" function to establish a preliminary ordering of clusters. Pseudotime values were determined by calculating Euclidean distances among cluster coordinates. Trajectory curves were fitted using the "smooth.spline" function based on pseudotime values and visualized with the "plotTrajectory" function. The resulting trajectory matrix was further used to create pseudotime heatmaps for motif activity, gene scores, inferred gene expression, and chromatin accessibility peaks using "plotTrajectoryHeatmap".

Integrated analysis of scATAC-seq and scRNA-seq data

Integration of scATAC-seq and scRNA-seq datasets was performed using Seurat v.3.2.0. Gene activity scores were inferred from scATAC-seq data by aggregating accessibility signals across gene bodies and 2 kb upstream of transcription start sites. The scRNA-seq data were then used as a reference to identify anchors in both datasets using the "FindTransferAnchors" function with CCA as the dimensional reduction method. These anchors enabled mapping of scATAC-seq profiles onto corresponding scRNA-seq cell identities, thereby facilitating annotation of chromatin-defined cell populations.

Cell culture, proliferation, and differentiation

Primary porcine myogenic cells (PPMCs) were isolated from

embryos obtained by caesarean section and transported to the laboratory in sterile PBS maintained at 4°C. Somite tissues were dissected using sterile instruments and cut into small fragments. Tissue pieces were digested in 0.3% collagenase type I at 37°C for 2 h with gentle agitation every 15 min to facilitate cellular release. The resulting suspension was filtered through a 40 μm cell strainer to remove undigested material and centrifuged at 500 ×*g* for 5 min at room temperature. The supernatant was discarded, and the pellet was resuspended in 10 mL of growth medium consisting of F12 supplemented with 10% fetal bovine serum (FBS, Gibco, USA) and 1% penicillin/streptomycin (PS, Corning, USA). Cells were plated in culture dishes and maintained at 37°C in a 5% CO_2 gas-jacketed incubator. After 12 h, the upper culture medium was discarded, followed by the addition of 1 mL of trypsin and incubation at 37°C for 3 min. Subsequently, 1 mL of growth medium was added to stop digestion. Cells were centrifuged at 500 ×*g* for 5 min at room temperature, resuspended in growth medium, and replated. After 45 min of incubation at 37°C, the supernatant containing enriched myogenic cells was transferred to a new culture dish. Medium was replaced every 2 days. When confluence reached approximately 90%, cells were passaged or cryopreserved for subsequent experiments.

C2C12, 3T3-L1, HEK-293T, and HepG2 cell lines were obtained from the American Type Culture Collection (ATCC). Cells were cultured in Dulbecco's Modified Eagle Medium (DMEM, Corning, USA) supplemented with 10% FBS and 1% PS. To induce myogenic differentiation, confluent cultures were transferred to DMEM/F12 containing 2% horse serum and maintained for 6–8 days with medium renewal every 2 days. All cell lines were maintained at 37°C in an incubator with 5% CO_2.

Gene overexpression

For *NTN5* and *LSAMP* overexpression vectors, coding sequences of the pig *NTN5* and *LSAMP* genes were inserted into the pcDNA3.1 expression vector (Invitrogen, USA). Cells were seeded into 6- or 12-well plates 12 h before transfection. Plasmids were introduced using Lipofectamine 3000 (Invitrogen, USA) according to manufacturer instructions.

Immunofluorescence

Cells were rinsed with PBS, fixed in 4% paraformaldehyde for 10 min, and washed three times with PBS. Permeabilization was performed using 0.5% TritonX-100 in PBS for 15 min, followed by blocking in 5% bovine serum albumin (BSA) for 30 min at room temperature. Primary antibodies were applied overnight at 4°C. After washing, cells were incubated with appropriate fluorescent secondary antibodies for 1 h at room temperature. Nuclei were counterstained with 4′,6-diamidino2-phenylindole (DAPI; 1:1 000 in PBS). Fluorescence images were captured using an inverted fluorescence microscope (Nikon, Japan). Primary antibodies included: anti-Ki67 (Abcam, UK, ab15580) and anti-fast myosin skeletal heavy chain (Abcam, UK, ab51263). Secondary antibodies included anti-rabbit IgG(H+L), F(ab')2 fragment conjugated to Alexa Fluor 488 (Cell Signaling Technology, USA, #4412) and anti-mouse IgG (H+L), F(ab')2 fragment conjugated to Alexa Fluor 555 (Cell Signaling Technology, USA, #4409).

Statistical analysis

All data are presented as mean±standard deviation (SD). Statistical analyses were conducted using GraphPad Prism v.8.0. Comparisons between two independent groups were performed using Student's *t*-test. Significance thresholds were defined as *: $P<0.05$, **: $P<0.01$, and ***: $P<0.001$.

RESULTS

Comparative cellular landscape of growth-restricted and normal porcine embryonic somites

To assess the cellular composition of embryonic somites under different developmental conditions, somite and myotome tissues were isolated from growth-restricted and phenotypically normal pig embryos at E21. Single-cell suspensions were subjected to 10x Genomics scRNA-seq (Figure 1A). After stringent quality control, 21 350 high-quality cells were retained for downstream analysis (Supplementary Figure S1A). Feature counts and total transcript counts exhibited strong concordance, with a correlation coefficient of 0.91 (Supplementary Figure S1B). Dimensionality reduction and unsupervised clustering resolved 20 transcriptionally distinct clusters (Figure 1B, C). Differential gene expression analysis combined with established lineage markers enabled annotation of 11 cell populations (Figure 1D, E). Marker bubble and violin plots validated the specificity and robustness of cell identity assignments (Figure 1F; Supplementary Figure S1D). Functional enrichment analysis of DEGs further characterized lineage-specific biological programs (Supplementary Figure S2). Notably, the myocyte-muscle cell cluster showed significant enrichment for skeletal muscle contraction and skeletal muscle cell differentiation pathways, whereas the myoblast cluster was predominantly associated with cell cycle-related processes, including mitotic cytokinesis and mitotic cell cycle. This functional partitioning aligned with established biological functions of these distinct myogenic cell populations during this developmental phase, validating the robustness of the single-cell clustering approach.

RNA velocity analysis provided dynamic insight into the developmental trajectories of each cell population (Figure 1G). Quantitative comparison of cellular composition between developmental groups revealed significant differences (Figure 1H). Growth-restricted embryos exhibited reduced proportions of osteogenic and myogenic populations, accompanied by a significantly higher proportion of neurogenic cells, including neurons and neuron stem cells. Uniform manifold approximation and projection (UMAP) visualization of marker-positive subsets independently substantiated these shifts in lineage distribution (Supplementary Figure S3), indicating impaired skeletal muscle development in growth-restricted embryos.

Comparison of myogenic progression in growth-restricted and normal embryos

To analyze lineage-specific alterations within the myogenic compartment, clusters annotated as myoblast and myocyte-muscle cell populations were isolated for further cluster analysis. Reclustering resolved 11 transcriptionally distinct subpopulations (Figure 2A, B), which were annotated into six biologically interpretable subclusters based on canonical marker expression (Figure 2C). Myogenic progenitors exhibited the highest expression of *Pax3*, while myoblast C1 and myoblast C2 were defined by expression of the muscle stem cell marker *Pax7* and myogenic regulatory factor *Myf5*. Myocytes also expressed the myogenic differentiation factor *MyoD* and skeletal myogenic cell marker *MyoG* (myogenin). Genes associated with fusion and maturation, including

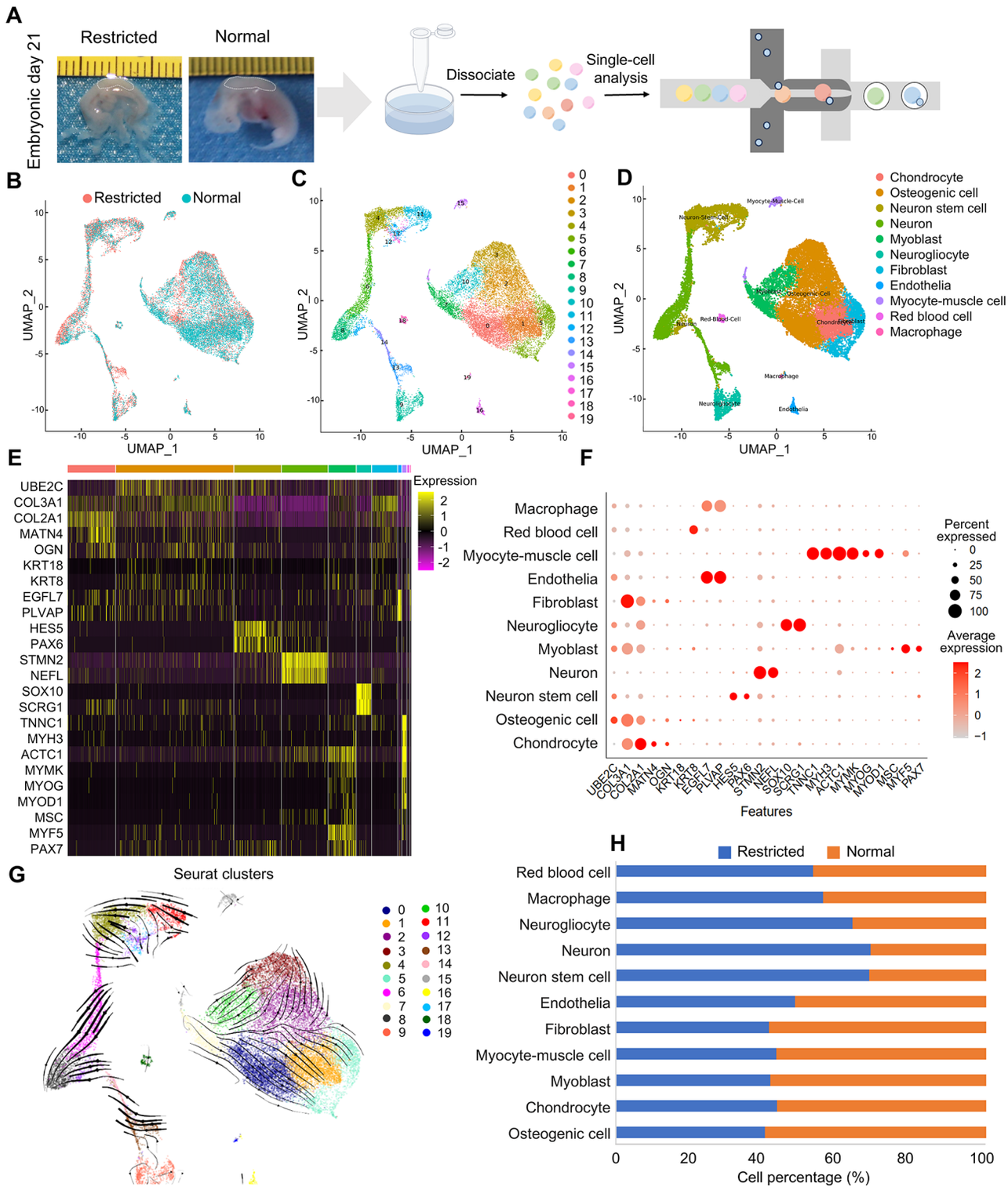

Figure 1 scRNA-seq identifies cellular heterogeneity in porcine embryonic somites

A: Schematic overview of the experimental workflow. Somite tissues were isolated from growth-restricted and phenotypically normal pig embryos at embryonic day 21 (E21). Tissues were dissociated into single-cell suspensions, and single-cell transcriptomes were captured using the 10x Genomics platform. Minimum scale of the ruler in the embryo image is 1 mm. B: Uniform manifold approximation and projection (UMAP) visualization of scRNA-seq data showing distribution of cell populations in pig embryos. C: Unsupervised clustering resolved 20 distinct cellular populations from embryonic somite tissue. D: Cell type annotation based on established marker gene expression identified osteogenic cells, chondrocytes, myoblasts, myocyte-muscle cells, fibroblasts, neurons, neuron stem cells, neurogliocytes, endothelial cells, red blood cells, and macrophages. E: Heatmap showing top 20 marker genes for each cluster. Yellow indicates high expression; dark red indicates low expression. F: Bubble-plot showing mean expression levels of canonical marker genes across 11 annotated cell populations. G: RNA velocity-based pseudotime trajectory depicting developmental relationships among the 20 cell clusters. H: Bar plot showing percentage of different cell types within each sample.

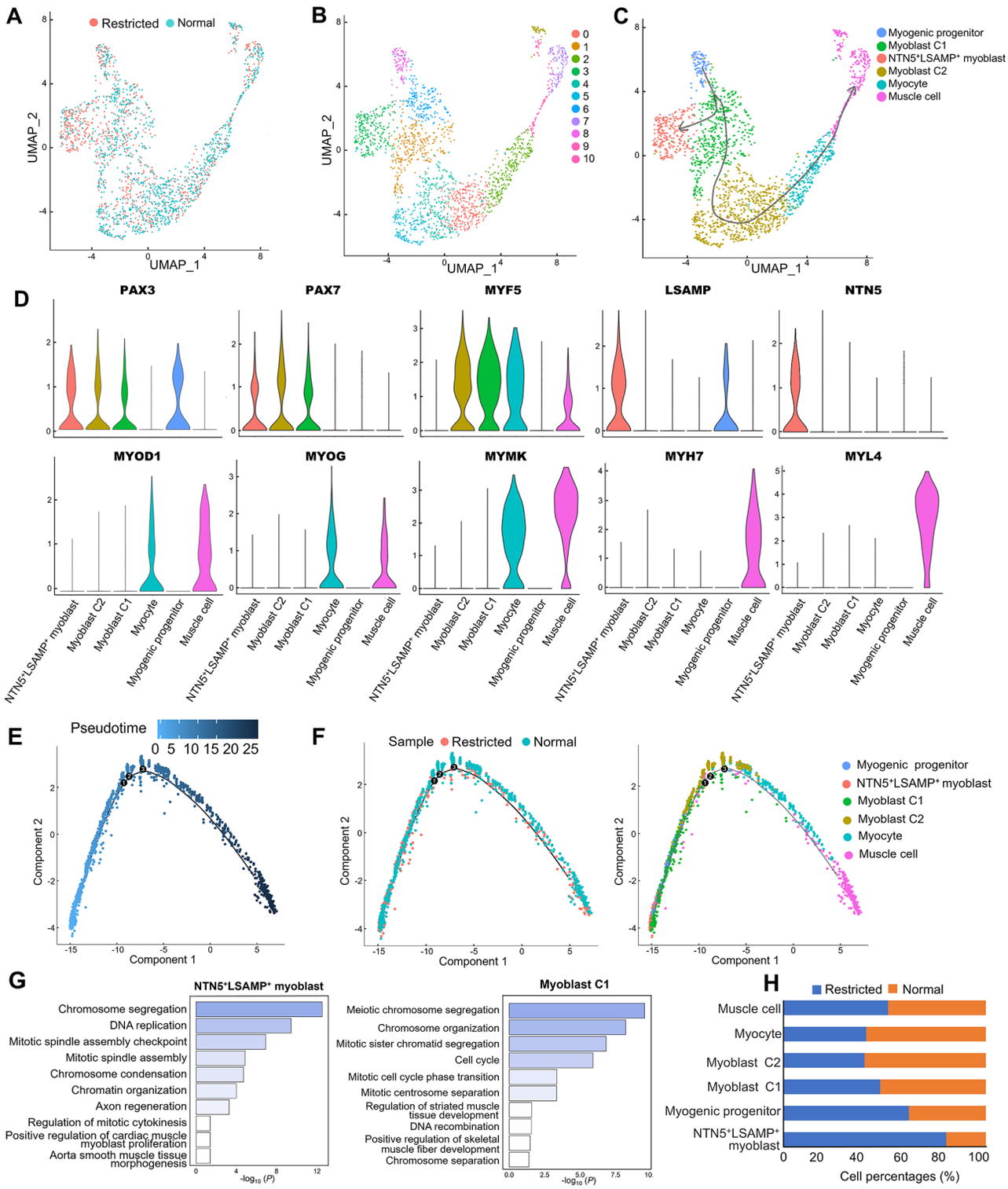

Figure 2 Comparison of myogenic progression between growth-restricted and normal embryos

A: UMAP of myogenic cells from both groups. B: Unsupervised reclustering of myogenic cells (including myoblasts and myocyte-muscle cells) identified 11 subclusters. C: Annotation of myogenic cells into six subclusters based on marker genes, including NTN5$^+$LSAMP$^+$ subpopulation enriched in Pax3$^+$ cells. D: Violin plots showing marker gene expression across subclusters. Colors represent subclusters described in panel C. E: Pseudotime trajectory colored by pseudotime values. F: Visualization of myogenic differentiation trajectory by cell origin (left) and cell identity (right). G: Gene Ontology (GO) analysis of DEGs highly expressed in NTN5$^+$LSAMP$^+$ myoblasts and myoblast C1. H: Bar plot showing percentage of annotated myogenic subtypes in each group.

MYMK, *MYH7*, and *MYL4*, were strongly enriched in muscle cells (Figure 2D). Among these subpopulations, a distinct cluster co-expressing *NTN5* and *LSAMP* emerged, identified as NTN5$^+$LSAMP$^+$ myoblasts.

Pseudotime reconstruction using Monocle2 resolved a predominantly unidirectional differentiation trajectory extending from progenitor states toward mature muscle cells, accompanied by a progressive decline in stemness signatures

(Figure 2E). Under canonical progression, myogenic progenitors ultimately transformed into muscle cells through myoblast C1, myoblast C2, and myocyte states (Figure 2F). In contrast, an alternative branch was identified in which myogenic progenitors advanced through myoblast C1 and diverged toward the NTN5$^+$LSAMP$^+$ myoblast state rather than continuing along the differentiation trajectory.

Quantitative comparison of subcluster proportions revealed marked compositional differences between developmental groups (Figure 2H). Growth-restricted embryos displayed a significant enrichment of NTN5$^+$LSAMP$^+$ myoblasts, whereas myoblast C2 and myocyte populations were more prevalent in normal embryos. UMAP visualization of marker-positive cells independently supported these distributional shifts (Supplementary Figure S4B). Functional enrichment analysis demonstrated that DEGs in NTN5$^+$LSAMP$^+$ myoblasts were predominantly associated with proliferative and neurogenic processes, including chromosome segregation, DNA replication, and axon regeneration. In contrast, myoblast C1 was enriched for pathways related to cell cycle progression and muscle development (Figure 2G; Supplementary Figure S4A). Collectively, these findings indicate that in growth-restricted embryos, myogenic progenitors are redirected into an aberrant differentiation trajectory, leading to accumulation at the NTN5$^+$LSAMP$^+$ myoblast state and consequent impairment of normal embryonic myogenesis.

NTN5 and LSAMP inhibit myogenic proliferation and differentiation

The NTN5$^+$LSAMP$^+$ myoblast population represented the largest myogenic subset in growth-restricted embryos, prompting investigation of the roles of *NTN5*, a member of the netrin axon guidance family, and *LSAMP* in myogenic regulation *in vitro*. Developmental expression dynamics were first examined using publicly available transcriptomic datasets spanning E33 to postnatal day 180 (P180) (Yang et al., 2019). Both *NTN5* and *LSAMP* displayed peak expression at E33, followed by marked down-regulation at E40, indicating preferential activity during early stages of embryonic myogenesis (Supplementary Figure S5E, F).

To define functional consequences, coding sequences of *NTN5* and *LSAMP* were overexpressed in C2C12 cells (Supplementary Figure S5A, B). Immunofluorescence staining demonstrated significant inhibition of both proliferative capacity and differentiation potential following overexpression (Figure 3A–C). Comparable inhibitory effects were observed in PPMCs (Figure 3D–F). Transcript analysis revealed significant reductions in cyclin D and Ki67 expression after NTN5 or LSAMP overexpression, supporting suppression of C2C12 proliferation (Supplementary Figure S5C). NTN5 overexpression further reduced the expression of MyoG and MYMX (Myomixer), indicating impaired differentiation and fusion (Supplementary Figure S5D). In contrast, LSAMP overexpression did not significantly alter MyoG or Myomixer expression; however, down-regulation of MyoD was observed, consistent with disruption of early myogenic processes (Supplementary Figure S5D). These molecular alterations are consistent with the observed phenotypic inhibition of myotube formation (Figure 3A–C).

Cell-type specificity was evaluated by assessing proliferation in additional cell lines. Overexpression of *NTN5* or *LSAMP* significantly inhibited proliferation of 3T3-L1 cells but did not exert measurable effects on HepG2 or HEK-293T cells (Supplementary Figure S6A–F), suggesting cell type-specific effects, with inhibition of proliferation varying depending on the cellular environment. Netrins are traditionally associated with axonal guidance via receptors such as DCC and UNC5, yet accumulating evidence supports broader roles in non-neuronal tissues (Cirulli & Yebra, 2007). Single-cell transcriptomic analysis indicated that NTN5$^+$LSAMP$^+$ myoblasts also expressed *Pax3* and *Pax7*, indicating a shift toward progenitor maintenance rather than differentiation. These findings align with previous research demonstrating that *NTN1* inhibits myoblast proliferation (Wang et al., 2019). However, suppression of differentiation by *NTN5* contrasts with activities reported for other netrin family members, such as *NTN1*, *NTN3*, and *NTN4* (Kang et al., 2004), highlighting functional divergence within the family during myogenesis. *LSAMP*, classically characterized as a limbic system-associated adhesion molecule mediating neurite outgrowth and synaptic specificity (Pimenta & Levitt, 2004; Sinopole et al., 2024), may disrupt myoblast fusion through interference with adhesion-dependent membrane dynamics. Inhibition of myogenic proliferation aligns with documented tumor-suppressive properties of LSAMP (Barøy et al., 2014; Wang et al., 2008). Accumulation of NTN5$^+$LSAMP$^+$ myoblast in growth-restricted embryos is therefore consistent with redirection of progenitors into a restrained or delayed differentiation state. Delayed differentiation under conditions of limited nutrient and oxygen availability may represent a transient adaptive response; however, sustained suppression of myogenic progression may compromise postnatal muscle development and predispose to reduced muscle mass or hypotonia.

ScATAC-seq reveals divergent chromatin accessibility profiles in growth-restricted and normal embryos

While epigenetic remodeling critically regulates lineage specification during embryogenesis, conventional scRNA-seq fails to resolve the underlying chromatin regulatory mechanisms. To define regulatory states associated with impaired myogenesis, scATAC-seq profiling was performed on growth-restricted and normal porcine embryos. ArchR-based quality control, batch correction, and dimensionality reduction generated high-resolution chromatin accessibility profiles from 18 146 nuclei (Supplementary Figure S7A–B). Subsequently, unsupervised clustering using the “Graphcluster” algorithm resolved 25 distinct chromatin-defined clusters characterized by differential accessibility peaks (Figure 4A; Supplementary Figure S7C). Exploration of the top differentially accessible loci revealed lineage-specific regulatory signatures. Clusters C17, C8, and C11 exhibited open chromatin at neural lineage regulators, including Sox2, CXCR4, and Pax6. Cluster C20 displayed enriched accessibility of loci associated with macrophage and endothelial identities, such as F11R, OLR1, and LTA. In contrast, clusters C3 and C23 retained accessible chromatin at canonical myogenic regulators, including MyoD and Myf5 (Supplementary Figure S7D), consistent with muscle lineage specification.

Integration of chromatin accessibility and transcriptional profiles was achieved through mutual nearest neighbor-based anchor mapping (Stuart et al., 2019), yielding 10 integrated cell populations (Figure 4B). Compositional analysis revealed enrichment of neurogenic populations, including neurons, neuron stem cells, and neurogliocytes, in growth-restricted embryos, accompanied by reduced representation of myogenic and osteogenic cells relative to normal embryos,

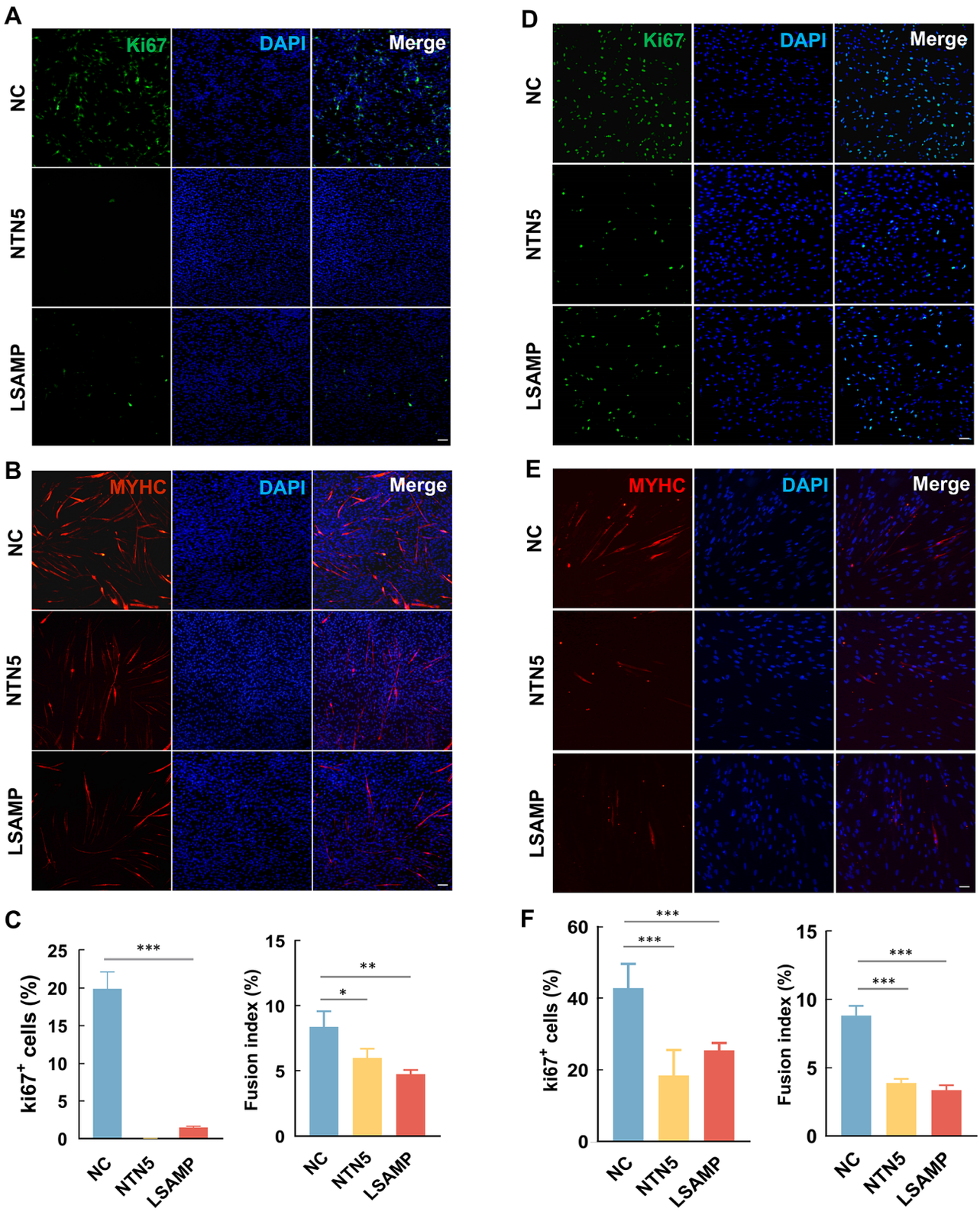

Figure 3 NTN5 and LSAMP are essential for myoblast proliferation and differentiation

A, B: Ki67 (A) and MyHC (B) immunofluorescence staining in C2C12 cells following *NTN5* or *LSAMP* overexpression. C: Quantification of Ki67-positive cells (left, *n*=3) and myonuclear fusion index (right, *n*=3). D, E: Representative Ki67 (D) and MyHC (E) immunofluorescence staining in pig primary myogenic cells following *NTN5* or *LSAMP* overexpression. F: Quantification of Ki67-positive cells (left) and myonuclear fusion index (right) (*n*=3). Myonuclear fusion index is defined as the percentage of nuclei within fused myotubes relative to the total number of nuclei. Data are presented as mean±SD. *: P<0.05; **: P<0.01; ***: P<0.001 (Student's *t*-test). Scale bars: 200 μm.

consistent with the scRNA-seq results (Figure 4C; Figure 1H). Enrichment heatmaps of lineage-defining accessible peaks further validated cluster annotation (Figure 4D, E).

The K-nearest neighbor (KNN) algorithm was employed to predict each myogenic cell type in the ATAC dataset, using single-cell transcriptomic data as a reference (Figure 5A, B).

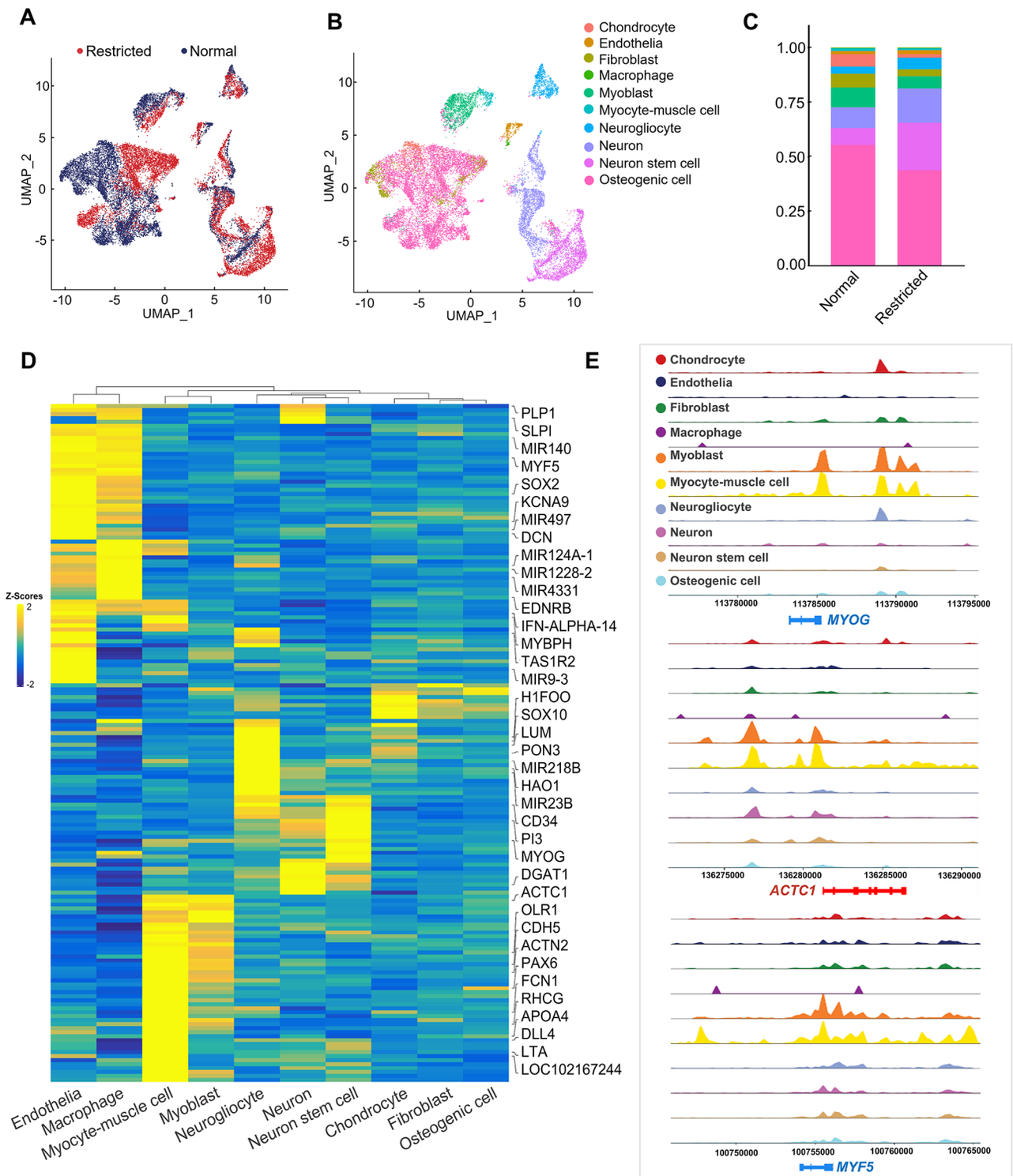

Figure 4 Single-cell chromatin accessibility profiling of porcine embryonic somites

A, B: UMAP visualization of scATAC-seq profiles from growth-restricted and normal pig embryo somites, colored by (A) sample and (B) annotated cell identity. C: Relative proportions of chromatin-defined cell clusters in normal and growth-restricted embryos. D: Heatmap showing top 20 up-regulated marker genes across all cell clusters. E: Chromatin accessibility landscape of canonical myogenic genes across all cell clusters.

This cross-modal mapping again demonstrated increased prevalence of NTN5^{+}LSAMP^{+} myoblasts in growth-restricted embryos (Figure 5C). Correlation between modalities revealed strong concordance across major myogenic subpopulations, with the highest correlation observed between myoblast C1 and myoblast C2 states (Figure 5D). Reduced concordance within progenitor populations likely reflects temporal asynchrony between chromatin accessibility dynamics and subsequent transcriptional activation during lineage commitment (Figure 5D). Global trajectory alignment further demonstrated high preservation of hierarchical ordering across scATAC-seq and scRNA-seq pseudotime reconstructions (Supplementary Figure S7E). Distinct enrichment of accessibility peaks within muscle cell and myocyte clusters indicated specialized regulatory architectures that distinguish these populations from other lineages

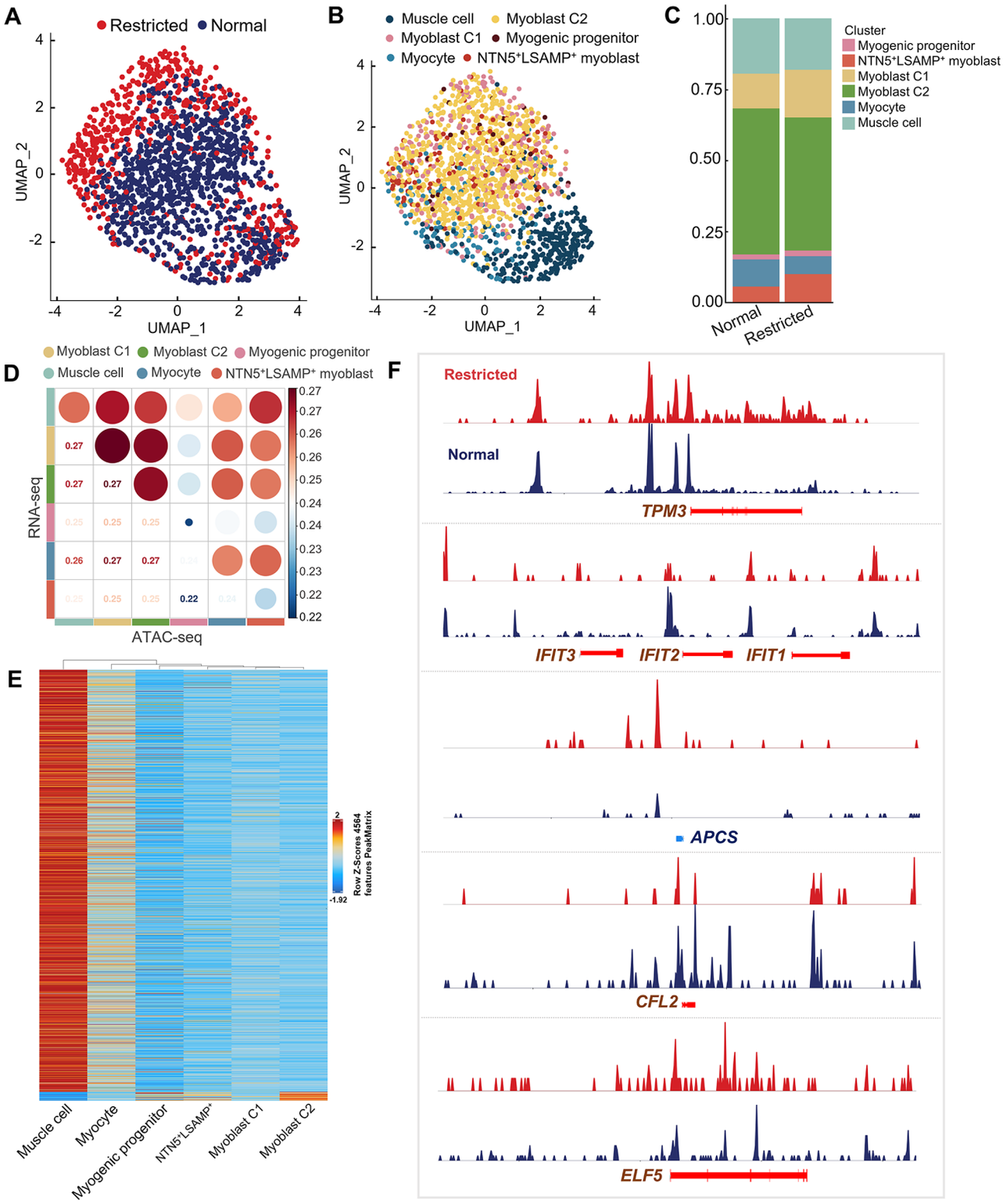

Figure 5 Single-cell chromatin accessibility analysis of myogenic cells

A, B: UMAP showing cross-modal mapping of scATAC-seq profiles onto scRNA-seq-annotated cell identities. C: Proportions of myogenic subclusters in normal and growth-restricted embryos. D: Correlation matrix comparing skeletal myogenic subpopulations between scRNA-seq and scATAC-seq datasets, with color intensity reflecting Pearson correlation coefficients. E: Heatmap of marker peak accessibility in myogenic subpopulations. Color intensity reflects peak accessibility. F: Differential chromatin accessibility landscape between growth-restricted and normal embryos.

(Figure 5E), consistent with lineage-restricted gene expression programs. Comparative analysis between developmental groups identified loci with significant differential accessibility, including key regulators such as TPM3, CFL2, and ELF5 (Figure 5F). Collectively, these data indicate that chromatin dysregulation perturbs embryonic axial patterning through aberrant transcriptional activation of morphogenetic regulators, ultimately culminating in myogenic developmental

arrest via disrupted spatial coordination of lineage specification programs.

Dysregulated signaling and metabolic reprogramming in growth-restricted embryos

To elucidate the mechanisms underlying impaired embryonic myogenesis, intercellular signaling dynamics were compared between growth-restricted and normal embryos. Analysis of ligand-receptor interactions across myogenic subclusters revealed that myoblast C1 exhibited the most extensive communication network among myogenic populations (Figure 6A). Differential analysis demonstrated significant alterations in outgoing signaling patterns across all myogenic subpopulations in growth-restricted embryos, whereas incoming signaling profiles remained largely unchanged (Figure 6A). Systematic profiling of intercellular signaling networks identified MSTN-mediated interactions between NTN5$^+$LSAMP$^+$ myoblasts and myogenic progenitors uniquely in growth-restricted embryos (Figure 6B, C; Supplementary Figure S8). Given the established inhibitory role of MSTN in myogenesis (McPherron et al., 1997), this aberrant signaling likely contributes to the impaired muscle development observed in growth-restricted embryos. Notably, IGF1-mediated interactions between NTN5$^+$LSAMP$^+$ myoblasts and myoblast C2 were also exclusively detected in growth-restricted embryos (Figure 6C), suggesting activation of stress-responsive or compensatory signaling circuits to support myogenic progression. Consistent with these observations, NTN5 overexpression in C2C12 cells significantly increased IGF1 and MSTN transcript levels (Supplementary Figure S5D), indicating that NTN5 regulates embryonic myogenesis through multiple mechanisms. In contrast, CXCL family-mediated autocrine and paracrine interactions among myoblast C2, myoblast C1 and muscle cell populations were selectively absent in growth-restricted embryos (Figure 6C; Supplementary Figure S8). This finding aligns with the established role of CXCL12 in regulating myogenic progenitor recruitment and maintenance (Gilbert et al., 2019). Additional ligand-receptor analyses revealed divergent activation patterns in developmental pathways, including Notch and Wnt signaling, between growth-restricted and normal embryos (Supplementary Figure S8).

To delineate the transcriptional regulatory programs driving myogenic heterogeneity, SCENIC was applied to reconstruct cell type-specific gene regulatory networks. Distinct transcription factor activity patterns were identified across myogenic subclusters. Notably, PRRX1 activity was significantly elevated in NTN5$^+$LSAMP$^+$ myoblasts (Figure 6D), the dominant myogenic population in growth-restricted embryos, consistent with reported inhibitory effects of PRRX1 in suppressing myogenic function (Guo et al., 2018). Concurrently, reduced activity of Myf5, MyoD, and MyoG within this subpopulation correlated with abnormal muscle developmental trajectories in growth-restricted embryos (Figure 6D).

Quantitative set analysis of gene expression (QuSAGE) identified pathway-level perturbations within specific cellular subpopulations (Figure 7A). Notably, the glycolysis and gluconeogenesis pathways were significantly down-regulated in NTN5$^+$LSAMP$^+$ myoblasts and in myoblast C2 from growth-restricted embryos relative to normal controls (Figure 7B). Insulin secretion-associated signatures also exhibited different patterns across subpopulations. In normal embryos, myoblast C2 displayed enhanced insulin secretion-related activity, suggesting a specific role in maintaining glucose homeostasis. Conversely, in growth-restricted embryos, muscle cell, myoblast C2, and myoblast C1 populations showed marked reductions in secretion activity, indicating metabolic dysfunction (Figure 7D). These findings suggest that altered IGF1-IGF1R interactions in growth-restricted embryos coexist with suppression of glycolytic flux and impaired insulin secretory capacity, consistent with reallocation of energy resources under pathological stress (Figure 6C; Figure 7B, D). Comparative pathway analysis further revealed significant down-regulation of TGF-β and Hippo signaling cascades, potentially disrupting proliferation-differentiation equilibrium and impairing tissue homeostasis (Figure 7C, E).

Collectively, these findings reveal coordinated disruption of signaling networks, transcriptional control, and metabolic homeostasis in developmentally retarded embryos, leading to impaired myogenic progression and compromised developmental maturation.

DISCUSSION

The molecular determinants underlying muscle hypoplasia in developmentally delayed embryos remain poorly understood. Integrated multi-omics analysis of porcine embryonic somites revealed a coordinated disruption of myogenic progression characterized by three interdependent pathological mechanisms: aberrant accumulation of differentiation-arrested NTN5$^+$LSAMP$^+$ progenitors, epigenetic restriction of cytoskeletal plasticity, and widespread perturbation of metabolic and signaling networks. These convergent abnormalities indicate that developmental delay arises from both intrinsic defects in progenitor lineage commitment and extrinsic microenvironmental disruptions.

Compared with normal embryos, the growth-restricted embryos exhibited a marked reduction in myogenic and osteogenic populations accompanied by expansion of neurogenic lineages. This imbalance is consistent with dysregulation of the canonical Wnt and Notch signaling axis, a central regulatory framework governing musculoskeletal versus neural fate decisions during somitogenesis (Aulehla et al., 2003; Dequéant et al., 2006; Dunty et al., 2008).

In this study, a distinct NTN5$^+$LSAMP$^+$ subpopulation was delineated and found to be markedly enriched in growth-restricted embryos, occupying an aberrant branch along the reconstructed pseudotime trajectory (Figure 2E). This spatial positioning within the differentiation continuum provides direct evidence of developmental arrest within the myogenic lineage. Members of the netrin family, including NTN5, guide cellular and axonal migration through interactions with UNC5 and DCC receptors during neural development (Engelkamp, 2002; Livesey, 1999; Rajasekharan & Kennedy, 2009). Beyond axon guidance, netrins coordinate organ morphogenesis by modulating directed migration and cytoskeletal architecture (Hinck, 2004) and have also been implicated in placental implantation processes (Kaya et al., 2023). Similarly, LSAMP primarily mediates intercellular adhesion and signaling and may influence tissue patterning through neuromodulatory pathways (Bregin et al., 2019). Functional validation assays demonstrated that *NTN5* and *LSAMP* inhibited proliferation and differentiation in both murine C2C12 cells and porcine primary myoblasts (Figure 3A–D), contrasting with canonical netrin-associated promotion of migration or fusion via DCC and UNC5 receptors (Carlsson et al., 1999; Kang et al., 2004;

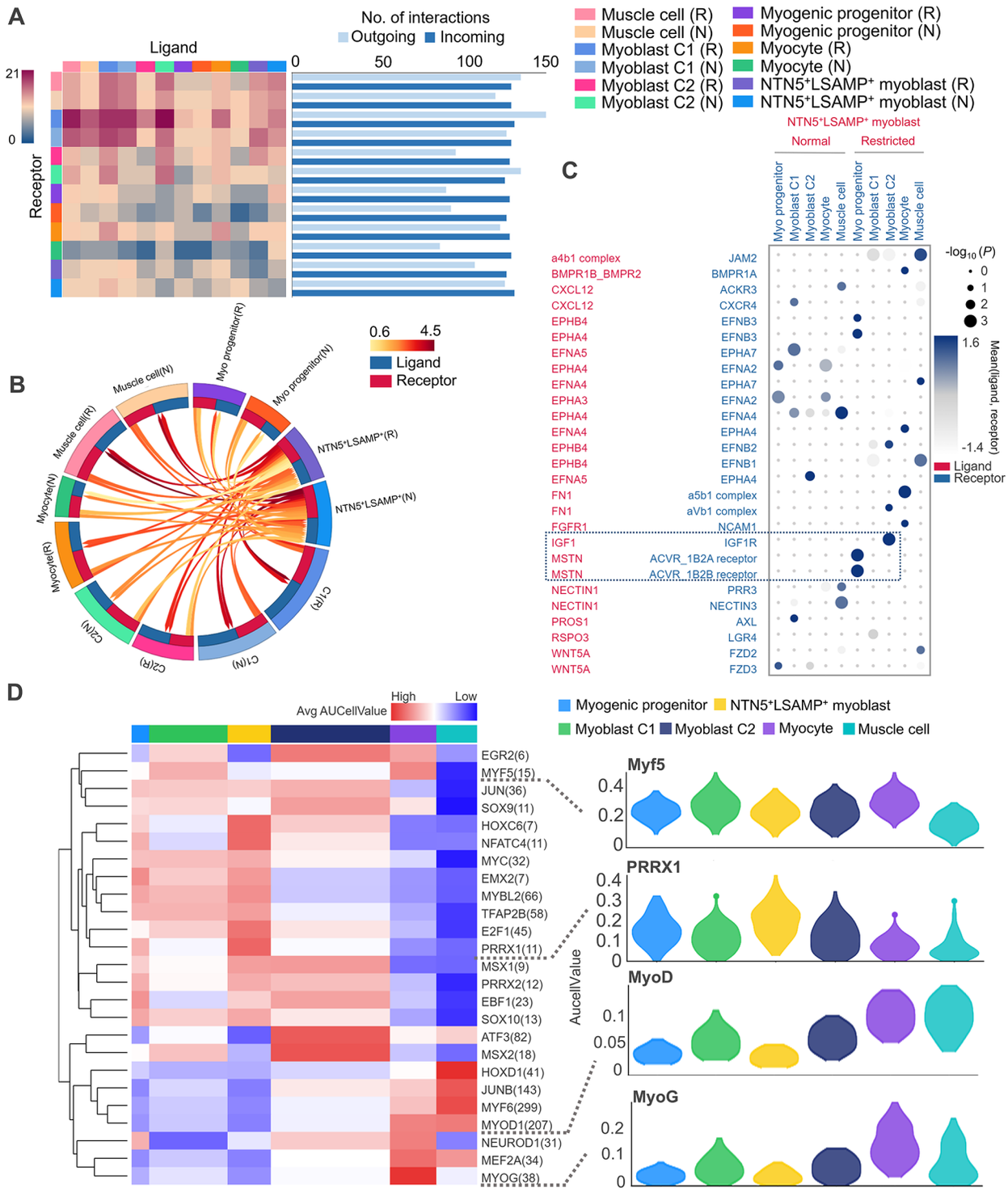

Figure 6 Differences in intercellular communication between growth-restricted and normal embryonic myogenic subpopulations

A: Heatmap (left) showing cell-cell interaction counts between normal (N) and growth-restricted (R) embryos, with color intensity indicating number of protein-protein interactions across cell clusters. Bar plot (right) showing number of output and input signals in normal and growth-restricted embryos. B: Interaction network between NTN5^{+}LSAMP^{+} myoblast clusters and other myogenic cell populations. C: Ligand-receptor interactions involving NTN5^{+}LSAMP^{+} myoblasts. Dot size indicates significance level; color represents interaction strength. D: Heatmap (left) showing average transcription factor regulatory activity across myogenic subpopulations, with module width representing number of cells. Violin plots (right) showing distribution of selected transcription factor activity.

Lindqvist et al., 2017). Mechanistically, *NTN5* may disrupt myogenic commitment by antagonizing NTN1-DCC signaling through competitive receptor interactions (Lejmi et al., 2008; Wang et al., 1999), whereas *LSAMP* may enforce proliferative quiescence via modulation of the β1-integrin/FAK pathway (Barøy et al., 2014; Kamranvar et al., 2022; Sun et al., 2019; Zhao et al., 2001). This multi-layered blockade collectively restricts expansion of functional myoblast pools, thereby

Figure 7 QuSAGE analysis reveals signaling pathway perturbations in growth-restricted embryos

A: Relative activation levels and statistical significance of gene sets across myogenic subpopulations. Color indicates activation status (red: active; blue: inactive), with darker hues representing higher intensity. Top annotation bar indicates myogenic subclusters derived from normal (N) and growth-restricted (R) embryos. B–E: Enrichment scores for individual gene sets. Significant results (FDR<0.05) are highlighted (orange, activation; blue, suppression), whereas non-significant results (FDR≥0.05) are shown in gray.

contributing to muscle hypoplasia. Proliferation assays further demonstrated that *NTN5* and *LSAMP* significantly inhibited the proliferation of 3T3-L1 fibroblasts, a widely recognized mesenchymal lineage model, while exerting negligible effects on HepG2 and HEK-293T cells. This lineage-restricted response is consistent with developmental origin, as both myogenic cells (Yang et al., 2013) and fibroblasts (Plikus et al., 2021) derive from mesenchymal progenitors. In

contrast, HepG2 cells represent a differentiated epithelial-derived hepatoma line (Aden et al., 1979; Dearfield et al., 1983) and HEK-293T cells originate from embryonic kidney epithelium transformed by SV40 large T antigen (Thomas & Smart, 2005). The observed differences in response to NTN5 and LSAMP may therefore reflect lineage-specific distribution of cognate receptors and downstream signaling components. Collectively, these observations support a model in which *NTN5* and *LSAMP* act as context-dependent regulators that constrain proliferation within mesenchymal-derived cell populations during embryonic development.

Differential chromatin accessibility at *TPM3*, *APCS*, and *CFL2* loci (Figure 5F) implies epigenetic dysregulation affecting cytoskeletal regulatory loci involved in myogenic maturation. Enhanced accessibility at tropomyosin-3 (*TPM3*) in growth-restricted embryos may reflect compensatory cytoskeletal remodeling (Huang et al., 2024; Lambert & Gussoni, 2023; Moraczewska, 2020; Sen et al., 2024). In contrast, reduced accessibility at cofilin-2 (*CFL2*), a key actin depolymerization factor essential for myoblast fusion, suggests impaired cytoskeletal reorganization capacity in growth-restricted embryos (Nguyen et al., 2020, 2021). Such opposing chromatin states are consistent with a restrictive epigenetic configuration that constrains cytoskeletal plasticity, potentially reinforcing the differentiation blockade associated with NTN5$^+$LSAMP$^+$ progenitor accumulation. Concomitant activation of IGF1-IGFR1 signaling in growth-restricted embryos may represent an ineffective compensatory response, analogous to feedback activation observed in insulin-resistant skeletal muscle (Abdul-Ghani & DeFronzo, 2010; Deshmukh, 2016). Loss of CXCL12-CXCR4 signaling, which is critical for stem cell niche maintenance, may further disrupt progenitor cell migration. In parallel, enhanced MSTN-ACVR signaling is consistent with potentiation of inhibitory cues that exacerbate differentiation failure (Ödemis et al., 2005; Puchert et al., 2016; Wei et al., 2015).

Regulatory network reconstruction using SCENIC demonstrated that transcriptional suppression of *MyoD* and *MyoG* in NTN5$^+$LSAMP$^+$ cells prevented activation of core myogenic regulatory programs. QuSAGE analysis further identified coordinated suppression of glycolysis alongside down-regulation of Hippo and TGF-β signaling pathways, indicating systemic metabolic dysregulation in growth-restricted embryos. This observed dysregulation aligns with established roles of Hippo and TGF-β signaling in metabolic control. Notably, Hippo signaling has been shown to regulate lipid metabolism through YAP-mediated mechanisms and cooperate with ChREBP in hepatic glucose utilization (Miao et al., 2023; Shu et al., 2020), while TGF-β signaling modulates glucose and lipid homeostasis via the AMPK/TGF-β1/Smad axis (Cai et al., 2023a). Integration of these pathways through AMPK-Hippo crosstalk provides a framework for coordinated control of energy homeostasis (Wang et al., 2015). Collectively, these findings support a mechanistic link between suppression of Hippo and TGF-β signaling pathways and the metabolic dysfunction observed in growth-restricted embryos. In parallel, activation of Notch1 signaling promotes maintenance of progenitor quiescence and restricts progression toward myogenic differentiation (Gioftsidi et al., 2022; Jo et al., 2022; Kashihara & Sadoshima, 2024; Koo & Guan, 2018).

CONCLUSIONS

Integrated multi-omics analysis identified the NTN5$^+$LSAMP$^+$ myoblast subpopulation as a central driver of myogenic arrest in developmentally delayed embryos. Coordinated disruption of non-canonical netrin signaling, chromatin accessibility, and metabolic dysregulation converged to impair lineage commitment and muscle differentiation. Inhibition of Hippo/TGF-β signaling, together with aberrant ligand-receptor interactions, further destabilized the balance between progenitor maintenance and differentiation. These findings offer novel insights into the pathogenesis of prenatal myogenesis and establish NTN5 and LSAMP as key regulators of skeletal muscle development, providing potential therapeutic targets for fetal growth disorders and livestock breeding.

DATA AVAILABILITY

The scRNA-seq and scATAC-seq data are available from the Science Data Bank (ScienceDB) under accession code 10.57760/sciencedb.29528, Sequence Read Archive (SRA) of the National Center for Biotechnology Information (NCBI) under BioProjectID PRJNA1336643, and Genome Sequence Archive (GSA) of the China National Center for Bioinformation (CNCB) under accession number PRJCA047145.

SUPPLEMENTARY DATA

Supplementary data to this article can be found online.

COMPETING INTERESTS

The authors declare that they have no competing interests.

AUTHORS' CONTRIBUTIONS

D.L.M. designed and conceived this project; R.X. and X.Y.W. analyzed the scRNA-seq and scATAC-seq data and performed immunofluorescence assays; Z.T.F. helped with scRNA-seq data analysis; Z.Y.L., L.P.P., and Q.S.Z. helped with plasmid extraction and cell culture; S.F.C. provided the normal embryo sequencing data; D.L.M., X.H.L., and Y.S.C. provided financial support, data discussions, and advice; R.X. and D.L.M. wrote the manuscript. All authors read and approved the final version of the manuscript.

REFERENCES

Abdul-Ghani MA, DeFronzo RA. 2010. Pathogenesis of insulin resistance in skeletal muscle. *Journal of Biomedicine & Biotechnology*, **2010**: 476279.

Aden DP, Fogel A, Plotkin S, et al. 1979. Controlled synthesis of HBsAg in a differentiated human liver carcinoma-derived cell line. *Nature*, **282**(5739): 615–616.

Aulehla A, Wehrle C, Brand-Saberi B, et al. 2003. *Wnt3a* plays a major role in the segmentation clock controlling somitogenesis. *Developmental Cell*, **4**(3): 395–406.

Barøy T, Kresse SH, Skårn M, et al. 2014. Reexpression of *LSAMP* inhibits tumor growth in a preclinical osteosarcoma model. *Molecular Cancer*, **13**: 93.

Bentzinger CF, Wang YX, Rudnicki MA. 2012. Building muscle: molecular regulation of myogenesis. *Cold Spring Harbor Perspectives in Biology*, **4**(2): a008342.

Bez Batti Angulski A, Hosny N, Cohen H, et al. 2023. Duchenne muscular dystrophy: disease mechanism and therapeutic strategies. *Frontiers in Physiology*, **14**: 1183101.

Bober E, Franz T, Arnold HH, et al. 1994. *Pax-3* is required for the development of limb muscles: a possible role for the migration of dermomyotomal muscle progenitor cells. *Development*, **120**(3): 603–612.

Bregin A, Mazitov T, Aug I, et al. 2019. Increased sensitivity to

psychostimulants and GABAergic drugs in Lsamp-deficient mice. *Pharmacology Biochemistry and Behavior*, **183**: 87–97.

Buckingham M, Relaix F. 2015. PAX3 and PAX7 as upstream regulators of myogenesis. *Seminars in Cell & Developmental Biology*, **44**: 115–125.

Butterfield RJ. 2019. Congenital muscular dystrophy and congenital myopathy. *Continuum*, **25**(6): 1640–1661.

Cai JL, Zhu YL, Li XP, et al. 2023a. Liposomal silybin improves glucose and lipid metabolisms in Type 2 diabetes mellitus complicated with non-alcoholic fatty liver disease via AMPK/TGF-β1/Smad signaling. *The Tohoku Journal of Experimental Medicine*, **261**(4): 257–265.

Cai SF, Hu B, Wang XY, et al. 2023b. Integrative single-cell RNA-seq and ATAC-seq analysis of myogenic differentiation in pig. *BMC Biology*, **21**(1): 19.

Carlsson L, Li Z, Paulin D, et al. 1999. Nestin is expressed during development and in myotendinous and neuromuscular junctions in wild type and Desmin knock-out mice. *Experimental Cell Research*, **251**(1): 213–223.

Chal J, Pourquié O. 2017. Making muscle: skeletal myogenesis *in vivo* and *in vitro*. *Development*, **144**(12): 2104–2122.

Cirulli V, Yebra M. 2007. Netrins: beyond the brain. *Nature Reviews Molecular Cell Biology*, **8**(4): 296–306.

De Micheli AJ, Spector JA, Elemento O, et al. 2020. A reference single-cell transcriptomic atlas of human skeletal muscle tissue reveals bifurcated muscle stem cell populations. *Skeletal Muscle*, **10**(1): 19.

Dearfield KL, Jacobson-Kram D, Brown NA, et al. 1983. Evaluation of a human hepatoma cell line as a target cell in genetic toxicology. *Mutation Research/Fundamental and Molecular Mechanisms of Mutagenesis*, **108**(1-3): 437–449.

Dequéant ML, Glynn E, Gaudenz K, et al. 2006. A complex oscillating network of signaling genes underlies the mouse segmentation clock. *Science*, **314**(5805): 1595–1598.

Deshmukh AS. 2016. Insulin-stimulated glucose uptake in healthy and insulin-resistant skeletal muscle. *Hormone Molecular Biology and Clinical Investigation*, **26**(1): 13–24.

Dunty Jr WC, Biris KK, Chalamalasetty RB, et al. 2008. Wnt3a/β-catenin signaling controls posterior body development by coordinating mesoderm formation and segmentation. *Development*, **135**(1): 85–94.

Emery AEH. 2002. The muscular dystrophies. *The Lancet*, **359**(9307): 687–695.

Engelkamp D. 2002. Cloning of three mouse *Unc5* genes and their expression patterns at mid-gestation. *Mechanisms of Development*, **118**(1-2): 191–197.

Findlay AR, Weihl CC. 2022. Genetic-based treatment strategies for muscular dystrophy and congenital myopathies. *Continuum*, **28**(6): 1800–1816.

Frontera WR, Ochala J. 2015. Skeletal muscle: a brief review of structure and function. *Calcified Tissue International*, **96**(3): 183–195.

Gilbert W, Bragg R, Elmansi AM, et al. 2019. Stromal cell-derived factor-1 (CXCL12) and its role in bone and muscle biology. *Cytokine*, **123**: 154783.

Gioftsidi S, Relaix F, Mourikis P. 2022. The Notch signaling network in muscle stem cells during development, homeostasis, and disease. *Skeletal Muscle*, **12**(1): 9.

Guo LJ, Huang WL, Chen B, et al. 2018. gga-mir-133a-3p regulates myoblasts proliferation and differentiation by targeting *PRRX1*. *Frontiers in Genetics*, **9**: 577.

Hinck L. 2004. The versatile roles of "axon guidance" cues in tissue morphogenesis. *Developmental Cell*, **7**(6): 783–793.

Huang K, Yang WJ, Shi MX, et al. 2024. The role of TPM3 in protecting cardiomyocyte from hypoxia-induced injury via cytoskeleton stabilization. *International Journal of Molecular Sciences*, **25**(12): 6797.

Jo YW, Park I, Yoo K, et al. 2022. Notch1 and Notch2 signaling exclusively but cooperatively maintain fetal myogenic progenitors. *Stem Cells*, **40**(11): 1031–1042.

Kamranvar SA, Rani B, Johansson S. 2022. Cell cycle regulation by integrin-mediated adhesion. *Cells*, **11**(16): 2521.

Kang JS, Yi MJ, Zhang W, et al. 2004. Netrins and neogenin promote myotube formation. *Journal of Cell Biology*, **167**(3): 493–504.

Kashihara T, Sadoshima J. 2024. Regulation of myocardial glucose metabolism by YAP/TAZ signaling. *Journal of Cardiology*, **83**(5): 323–329.

Kaya S, Turhan U, Dağ I. et al. 2023. Association of maternal serum Netrin-1 and Netrin-4 levels with placenta accreta spectrum. *European Review for Medical and Pharmacological Sciences*, **27**(10): 4594–4600.

Koo JH, Guan KL. 2018. Interplay between YAP/TAZ and Metabolism. *Cell Metabolism*, **28**(2): 196–206.

Lambert MR, Gussoni E. 2023. Tropomyosin 3 (TPM3) function in skeletal muscle and in myopathy. *Skeletal Muscle*, **13**(1): 18.

Lejmi E, Leconte L, Pédron-Mazoyer S, et al. 2008. Netrin-4 inhibits angiogenesis via binding to neogenin and recruitment of Unc5B. *Proceedings of the National Academy of Sciences of the United States of America*, **105**(34): 12491–12496.

Lindqvist J, Torvaldson E, Gullmets J, et al. 2017. Nestin contributes to skeletal muscle homeostasis and regeneration. *Journal of Cell Science*, **130**(17): 2833–2842.

Livesey FJ. 1999. Netrins and netrin receptors. *Cellular and Molecular Life Sciences CMLS*, **56**(1-2): 62–68.

Lunney JK, Van Goor A, Walker KE, et al. 2021. Importance of the pig as a human biomedical model. *Science Translational Medicine*, **13**(621): eabd5758.

McGinnis CS, Murrow LM, Gartner ZJ. 2019. DoubletFinder: Doublet Detection in Single-Cell RNA Sequencing Data Using Artificial Nearest Neighbors. *Cell systems*, **8**(4): 329–337.

McPherron AC, Lawler AM, Lee SJ. 1997. Regulation of skeletal muscle mass in mice by a new TGF-beta superfamily member. *Nature*, **387**(6628): 83–90.

Miao DJ, Wang Q, Shi J, et al. 2023. N6-methyladenosine-modified *DBT* alleviates lipid accumulation and inhibits tumor progression in clear cell renal cell carcinoma through the ANXA2/YAP axis-regulated Hippo pathway. *Cancer Communications*, **43**(4): 480–502.

Moraczewska J. 2020. Thin filament dysfunctions caused by mutations in tropomyosin Tpm3.12 and Tpm1.1. *Journal of Muscle Research and Cell Motility*, **41**(1): 39–53.

Nguyen MT, Min KH, Kim D, et al. 2020. CFL2 is an essential mediator for myogenic differentiation in C2C12 myoblasts. *Biochemical and Biophysical Research Communications*, **533**(4): 710–716.

Nguyen MT, Min KH, Lee W. 2021. Palmitic acid-induced miR-429-3p impairs myoblast differentiation by downregulating CFL2. *International Journal of Molecular Sciences*, **22**(20): 10972.

Ödemis V, Lamp E, Pezeshki G, et al. 2005. Mice deficient in the chemokine receptor CXCR4 exhibit impaired limb innervation and myogenesis. *Molecular and Cellular Neuroscience*, **30**(4): 494–505.

Osorio D, Cai JJ. 2021. Systematic determination of the mitochondrial proportion in human and mice tissues for single-cell RNA-sequencing data quality control. *Bioinformatics*, **37**(7): 963–967.

Parker MH, Seale P, Rudnicki MA. 2003. Looking back to the embryo: defining transcriptional networks in adult myogenesis. *Nature Reviews Genetics*, **4**(7): 497–507.

Picard B, Lefaucheur L, Berri C, et al. 2002. Muscle fibre ontogenesis in farm animal species. *Reproduction Nutrition Development*, **42**(5): 415–431.

Pimenta AF, Levitt P. 2004. Characterization of the genomic structure of the mouse limbic system-associated membrane protein (*Lsamp*) gene. *Genomics*, **83**(5): 790–801.

Plikus MV, Wang XJ, Sinha S, et al. 2021. Fibroblasts: origins, definitions, and functions in health and disease. *Cell*, **184**(15): 3852–3872.

Pownall ME, Gustafsson MK, Emerson Jr CP. 2002. Myogenic regulatory factors and the specification of muscle progenitors in vertebrate embryos. *Annual Review of Cell and Developmental Biology*, **18**: 747–783.

Puchert M, Adams V, Linke A, et al. 2016. Evidence for the involvement of the CXCL12 system in the adaptation of skeletal muscles to physical exercise. *Cellular Signalling*, **28**(9): 1205–1215.

Qiu XJ, Mao Q, Tang Y, et al. 2017. Reversed graph embedding resolves complex single-cell trajectories. *Nature Methods*, **14**(10): 979–982.

Rajasekharan S, Kennedy TE. 2009. The netrin protein family. *Genome Biology*, **10**(9): 239.

Relaix F, Montarras D, Zaffran S, et al. 2006. Pax3 and Pax7 have distinct and overlapping functions in adult muscle progenitor cells. *Journal of Cell Biology*, **172**(1): 91–102.

Schiaffino S, Dyar KA, Ciciliot S, et al. 2013. Mechanisms regulating skeletal muscle growth and atrophy. *The FEBS Journal*, **280**(17): 4294–4314.

Schubert FR, Tremblay P, Mansouri A, et al. 2001. Early mesodermal phenotypes in *splotch* suggest a role for *Pax3* in the formation of epithelial somites. *Developmental Dynamics*, **222**(3): 506–521.

Seale P, Sabourin LA, Girgis-Gabardo A, et al. 2000. Pax7 is required for the specification of myogenic satellite cells. *Cell*, **102**(6): 777–786.

Sen B, Xie ZH, Thomas MD, et al. 2024. Nuclear actin structure regulates chromatin accessibility. *Nature Communications*, **15**(1): 4095.

Shu ZP, Yi GW, Deng S, et al. 2020. Hippo pathway cooperates with ChREBP to regulate hepatic glucose utilization. *Biochemical and Biophysical Research Communications*, **530**(1): 115–121.

Sinopole KW, Babcock K, Dobi A, et al. 2024. A review of limbic system-associated membrane protein in tumorigenesis. *Biomedicines*, **12**(11): 2590.

Stirm M, Fonteyne LM, Shashikadze B, et al. 2022. Pig models for Duchenne muscular dystrophy -from disease mechanisms to validation of new diagnostic and therapeutic concepts. *Neuromuscular Disorders*, **32**(7): 543–556.

Stuart T, Butler A, Hoffman P, et al. 2019. Comprehensive integration of single-cell data. *Cell*, **177**(7): 1888–1902. e21.

Stuart T, Satija R. 2019. Integrative single-cell analysis. *Nature Reviews Genetics*, **20**(5): 257–272.

Subramanian A, Alperovich M, Yang YM, et al. 2022. Biology-inspired data-driven quality control for scientific discovery in single-cell transcriptomics. *Genome Biology*, **23**(1): 267.

Sun J, Zhou Y, Ye ZY, et al. 2019. Transforming growth factor-β1 stimulates mesenchymal stem cell proliferation by altering cell cycle through FAK-Akt-mTOR pathway. *Connective Tissue Research*, **60**(4): 406–417.

Tajbakhsh S. 2009. Skeletal muscle stem cells in developmental versus regenerative myogenesis. *Journal of Internal Medicine*, **266**(4): 372–389.

Thomas P, Smart TG. 2005. HEK293 cell line: a vehicle for the expression of recombinant proteins. *Journal of Pharmacological and Toxicological Methods*, **51**(3): 187–200.

Uapinyoying P, Hogarth M, Battacharya S, et al. 2023. Single-cell transcriptomic analysis of the identity and function of fibro/adipogenic progenitors in healthy and dystrophic muscle. *iScience*, **26**(8): 107479.

Wang H, Copeland NG, Gilbert DJ, et al. 1999. Netrin-3, a mouse homolog of human NTN2L, is highly expressed in sensory ganglia and shows differential binding to netrin receptors. *The Journal of Neuroscience*, **19**(12): 4938–4947.

Wang L, Hauser ER, Shah SH, et al. 2008. Polymorphisms of the tumor suppressor gene *LSAMP* are associated with left main coronary artery disease. *Annals of Human Genetics*, **72**(Pt 4): 443–453.

Wang LG, Zhao LL, Zhang LC, et al. 2019. *NTN1* affects porcine intramuscular fat content by affecting the expression of myogenic regulatory factors. *Animals*, **9**(9): 609.

Wang WQ, Xiao ZD, Li X, et al. 2015. AMPK modulates Hippo pathway activity to regulate energy homeostasis. *Nature Cell Biology*, **17**(4): 490–499.

Wei LP, Zhang B, Cao WW, et al. 2015. Inhibition of CXCL12/CXCR4 suppresses pulmonary arterial smooth muscle cell proliferation and cell cycle progression via PI3K/Akt pathway under hypoxia. *Journal of Receptors and Signal Transduction*, **35**(4): 329–339.

Xu DD, Wan BY, Qiu K, et al. 2023. Single‐cell RNA‐sequencing provides insight into skeletal muscle evolution during the selection of muscle characteristics. *Advanced Science*, **10**(35): 2305080.

Yang B, Zheng JH, Zhang YY. 2013. Myogenic differentiation of mesenchymal stem cells for muscle regeneration in urinary tract. *Chinese Medical Journal*, **126**(15): 2952–2959.

Yang YL, Zhu M, Fan XH, et al. 2019. Developmental atlas of the RNA editome in *Sus scrofa* skeletal muscle. *DNA Research*, **26**(3): 261–272.

Zhang YX, Wang JK, Yu C, et al. 2022. Advances in single-cell sequencing and its application to musculoskeletal system research. *Cell Proliferation*, **55**(1): e13161.

Zhao JH, Pestell R, Guan JL. 2001. Transcriptional activation of cyclin D1 promoter by FAK contributes to cell cycle progression. *Molecular Biology of the Cell*, **12**(12): 4066–4077.

Zhou H, Lian CJ, Wang TT, et al. 2019. *MET* mutation causes muscular dysplasia and arthrogryposis. *EMBO Molecular Medicine*, **11**(3): e9709.